31P MAS NMR and DFT study of crystalline phosphate matrices

Laura Martel, Attila Kovacs, Karin Popa, Damien Bregiroux, Thibault Charpentier

^{31}P MAS NMR and DFT study of crystalline phosphate matrices

Laura Martel[1]*, Attila Kovács[1], Karin Popa[1], Damien Bregiroux[2] and Thibault Charpentier[3]

[1]European Commission, Joint Research Centre (JRC), Postfach 2340, D-76125 Karlsruhe, Germany.
[2]Sorbonne Université, CNRS, Chimie de la Matière Condensée de Paris, LCMCP, F-75005 Paris, France.
[3]NIMBE, CEA, CNRS, Université Paris-Saclay, CEA Saclay 91191 Gif-sur-Yvette, France.

*laura.martel@ec.europa.eu

Abstract

We present the study of the phosphorus local environment by using ^{31}P MAS NMR in a series of seven double monophosphates $M^{II}M^{IV}(PO_4)_2$ (M^{II} and M^{IV} being divalent and tetravalent cations, respectively) of yavapaiite and low-yavapaiite type crystal structures. Solid-state and cluster DFT calculations were found to be efficient for predicting the ^{31}P isotropic chemical shift and chemical shift anisotropy. To achieve this performance, however, a proper computational optimisation of the experimental structural data was required. From the three optimisation methods tested, the full optimisation provided the best reference structure for the calculation of the NMR parameters of the studied phosphates. Also, a better prediction of the chemical shifts was possible by using a correction to the GIPAW calculated shielding.

Keywords: Yavapaiite; phosphates; ^{31}P NMR; DFT calculations; cluster model.

Graphical abstract

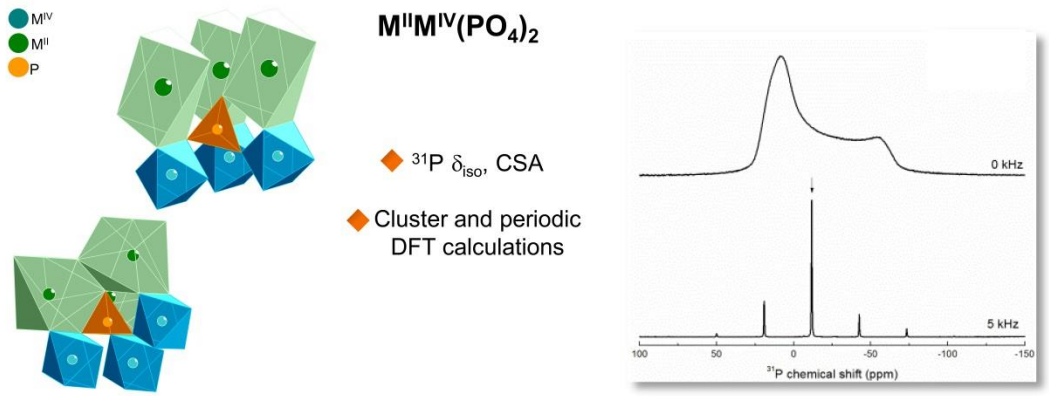

1. Introduction

Crystalline phosphates have aroused a lot of interest in the research community due to their numerous useful properties as ionic conductors[1], catalysts and ion exchangers[2] or luminescent materials and UV-emitting X-ray phosphors[3,4,5,6,7]. Most importantly, thanks to their structural and chemical stability, crystalline phosphates such as monazite, apatite or double monophosphates have been considered as matrices for immobilization of nuclear waste.[8,9,10,11,12,13,14,15,16,17,18,19,20,21,22] Even though the chemistry of double monophosphates has been studied in detail,[23,24] to our knowledge, the phosphorous local environment using ^{31}P solid-state NMR has not yet been probed. The efficiency of NMR in characterising the local environment of various nuclei has been demonstrated previously[25,26,27] and can therefore be extended to the titled systems. Our present aim is to analyse the local structure around the P atom in such diamagnetic phosphates via density functional theory (DFT) calculations. This knowledge can serve as basis for the understanding of the more complex NMR shifts of phosphates containing actinide or rare-earth cations. Indeed, as the NMR signals,[28,29] are influenced by the paramagnetic interactions,[30,31,32] the use of the cluster model can successfully help in the prediction of the paramagnetic shifts as shown in our recent study[33] on the $La_xEu_{1-x}PO_4$ series in which an $LaPO_4$ cluster was make. This approach was also applied by other authors in lithium batteries and is very promising.[34]

Here, we present the ^{31}P NMR spectra of selected crystalline structures of the type yavapaiite (*C2/m*)[35,36] ($BaHf(PO_4)_2$, $BaSn(PO_4)_2$, $BaGe(PO_4)_2$, $BaZr(PO_4)_2$, $BaTi(PO_4)_2$ and *β*-$SrGe(PO_4)_2$) and low-yapavaiite (*C2/c*) ($CaGe(PO_4)_2$[37]). The computational work was extended to other monophosphates for which experimental data are available in the literature: $LaPO_4$,[38,39] $AlPO_4$[40,41,42], $Si_5O(PO_4)_6$[43] and $Ge_5O(PO_4)_6$[44]. We probe several structure models used as basis for the NMR calculations. Beyond the experimental structure three computationally relaxed solid-state structures and two (molecular) cluster models were tested. We show the optimisation effects on the experimental crystalline structures and how the NMR parameters can be predicted by means of solid-state and molecular quantum chemical codes utilizing density functional theory (DFT).

2. Methods

2.1. *Synthesis*

The investigated $M^{II}M^{IV}(PO_4)_2$ compounds were obtained by solid-state reactions by mixing stoichiometric amounts of M^{II}- oxides or carbonates (Prolabo, Aldrich or Johnson Mattey) with $M^{IV}O_2$ and $NH_4H_2PO_4$/$(NH_4)_2HPO_4$. The powders were grounded and fired slowly. More details about the process are presented in Refs. 18, 23, 37, 45, 46, 47. All these crystalline phases[23] were checked by powder XRD and determined to be single-phased except for $CaGe(PO_4)_2$ in which the presence of $CaGe_4(PO_4)_6$ and $Ca_2P_2O_7$ were revealed by X-ray diffraction as small impurities (~4%).

2.2. *NMR measurements*

All ^{31}P NMR spectra (MAS and static) were collected at a Larmor frequency of 162.06 MHz (magnetic field 9.4 T) on a Bruker Avance III WB spectrometer using a Bruker 4mm MAS probe. Powder samples were spun at slow spinning rates of 2, 3 and 5 kHz in order to obtain the spinning sidebands pattern to extract the chemical shift anisotropy (CSA) parameters. Spectra were acquired using a 90° pulse of 7.8 μs in length (radiofrequency field of 32 kHz). The recycle delays used to have the full recovery of the magnetization were: 200 s for $BaHf(PO_4)_2$ and $BaSn(PO_4)_2$, 1000 s for $BaZr(PO_4)_2$, 1500 s for $BaTi(PO_4)_2$, 2200 s $CaGe(PO_4)_2$, 3000 s for $BaGe(PO_4)_2$ and β-$SrGe(PO_4)_2$. The spectra were referenced with respect to an external sample of liquid H_3PO_4 (0 ppm). The data were fitted using the DMfit software[48] and the CSA parameters were extracted using the "*CSA MAS model*".

2.3. *Solid-state DFT calculations*

Solid-state first-principles calculations of the NMR parameters were performed using the Quantum Espresso (QE)[49] package which relies on a pseudopotential plane-wave expansion formalism of DFT. The ^{31}P NMR parameters were computed using the gauge including projector augmented wave approach (GIPAW)[50,51] formalisms and the generalized gradient approximation (GGA) PBE functional[52]. Core electrons were described by norm-conserving Trouiller−Martins pseudopotentials[53] available in the QE library (Al, Ba, Ge, Hf, La, O, P, Si, Sn, Sr, Zr)[54], or downloaded from Davide Ceresoli's website[55](Ca) or generated with the *atomic* code[56] (Hf, Ti, Zr) (Table S1). For all calculations with QE, an optimized kinetic energy cutoff of 100 Ry and optimized Monkhorst–Pack grids given in Table S2 were selected. The data for $BaSn(PO_4)_2$ are given as an example in Table S3.

The calculated magnetic shielding parameters and σ_{iso} are defined by the Haeberlen convention[57,58,59] $|\sigma_{33} - \sigma_{iso}| > |\sigma_{11} - \sigma_{iso}| > |\sigma_{22} - \sigma_{iso}|$ with $\sigma_{iso} = \frac{1}{3}(\sigma_{11} + \sigma_{22} + \sigma_{33})$.

The axiality of the CSA tensor is defined by $\Delta_{CSA} = \sigma_{33} - \sigma_{iso}$ and its asymmetry by $\eta_{CSA} = \frac{\sigma_{22}-\sigma_{11}}{\sigma_{33}-\sigma_{iso}}$. The same convention was followed to extract the δ_{ii} parameters (i.e. $\Delta_{CSA} = \delta_{33} - \delta_{iso}$ and $\eta_{CSA} = \frac{\delta_{22}-\delta_{11}}{\delta_{33}-\delta_{iso}}$.).

2.4. *Cluster DFT calculations*

The ^{31}P magnetic shieldings of the target compounds were calculated by means of the cluster approach using the Gaussian 09 (G09) software[60]. The model structures (to be discussed later) were subjected to partial geometry optimisations in which the hydrogen atoms were relaxed while the heavy-atom core of the clusters was kept fix. We note that a full optimisation (governed by the hydrogen bonding interactions between close lying OH groups) would destroy the crystal character of the model. For these partial geometry optimisations valence double-zeta basis sets were used: the standard 6-31G** for the light P, O, H, Al, Ca, Si, Ge, Ti atoms, and the relativistic effective core potentials of Hay and Wadt (LANL2DZ): Sr, Ba, Sn,[61] and La, Zr, Hf[62]for the heavier metals.

All calculations were performed using the B3LYP[63,64] exchange-correlation functional and the PBE functional[52]. Dunning's correlation-consistent cc-pVTZ basis sets were utilised for the light atoms O, H;[65] Al, Si, P;[66] Ca;[67] Ge;[68] Ti[69]. For the heavier metals, the following small-core quasi-relativistic pseudopotentials and contracted valence basis sets of the Stuttgart group were used:[70],[71] Sr, ECP28MWB with 6s6p5d/4s4p2d;[72] Ba, ECP46MWB with 6s6p5d1f/4s4p2d;[70] Sn, ECP28MDF with 12s11p9d1f/5s4p3d1f;[73,74] Zr, ECP28MDF with 41s37s25d2f1g/5s5p4d2f1g;[75] Hf, ECP60MDF with 41s37s25d2f1g/5s5p4d2f1g[76] contraction schemes and La, ECP28MWB (the number meaning the core electrons replaced by the potential) with a 14s13p10d8f6g/10s8p5d4f3g contraction scheme. NMR calculations on the cluster structures were carried out using in conjunction with the pseudopotentials and basis sets applied in the B3LYP cluster calculations. The magnetic shieldings were calculated with the Gauge-Independent Atomic Orbital (GIAO) formalism.[77]

3. Results and discussions

3.1. *Crystalline structures of the $M^{II}M^{IV}(PO_4)_2$ phases*

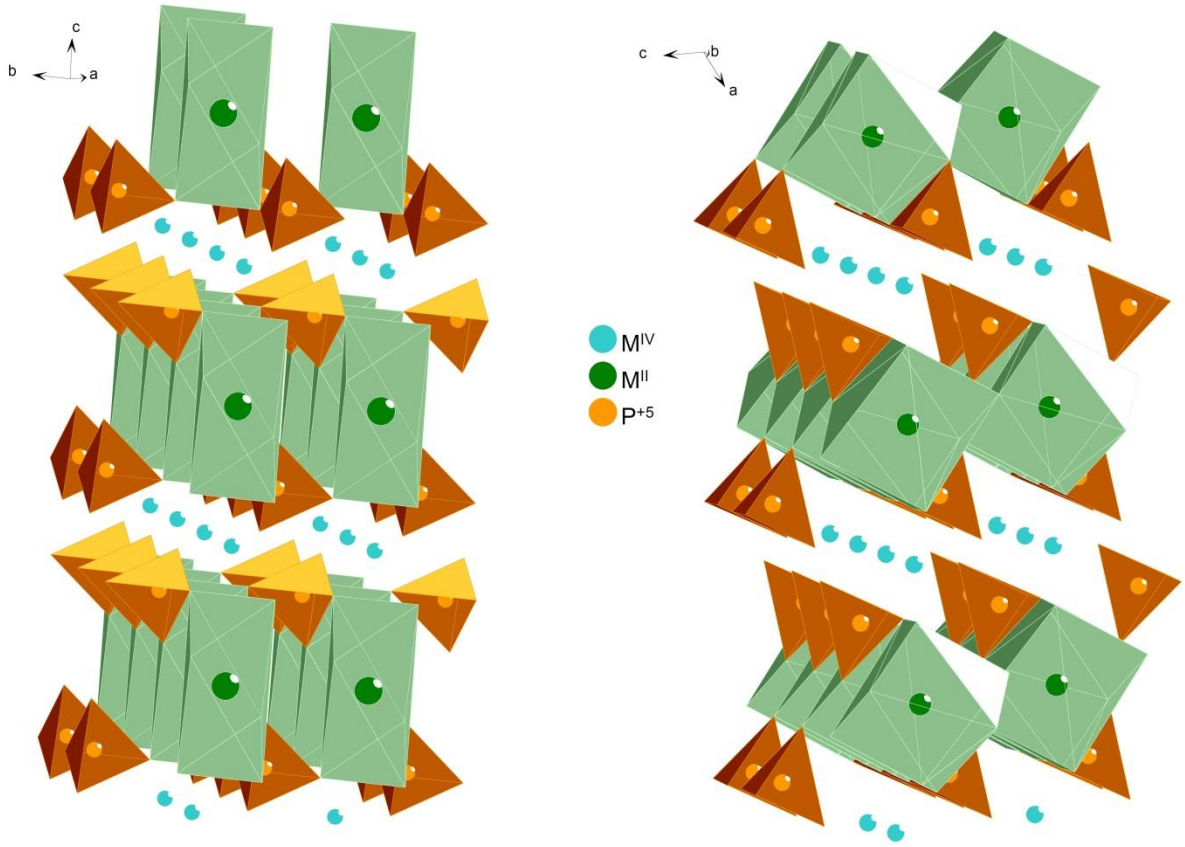

Figure 1: Crystalline structure of a) the yavapaiites and b) the low-yavapaiites. The M^{IV} cations have an octahedral coordination for the two structures.

In Figure 1 the two crystalline structures of the $M^{II}M^{IV}(PO_4)_2$ are presented. The yavapaiite crystalline structures the M^{IV} cations have an octahedral coordination and are corner-linked to six separate phosphate tetrahedra through the oxygen atoms, forming two different sheets. In between these sheets, a layer of 10-coordinated M^{II} cations is located, being also linked to the PO_4 units.[78] The low-yavapaiite structure can be described as a distorted yavapaiite with a double lattice along the a-axis. Compared to the yavapaiite, the tetravalent cations remain in an octahedral environment, whereas the 10-coordination of the divalent cations decreases to eight (capped with 2 additional oxygen atoms).[23]

3.2. *^{31}P NMR spectra*

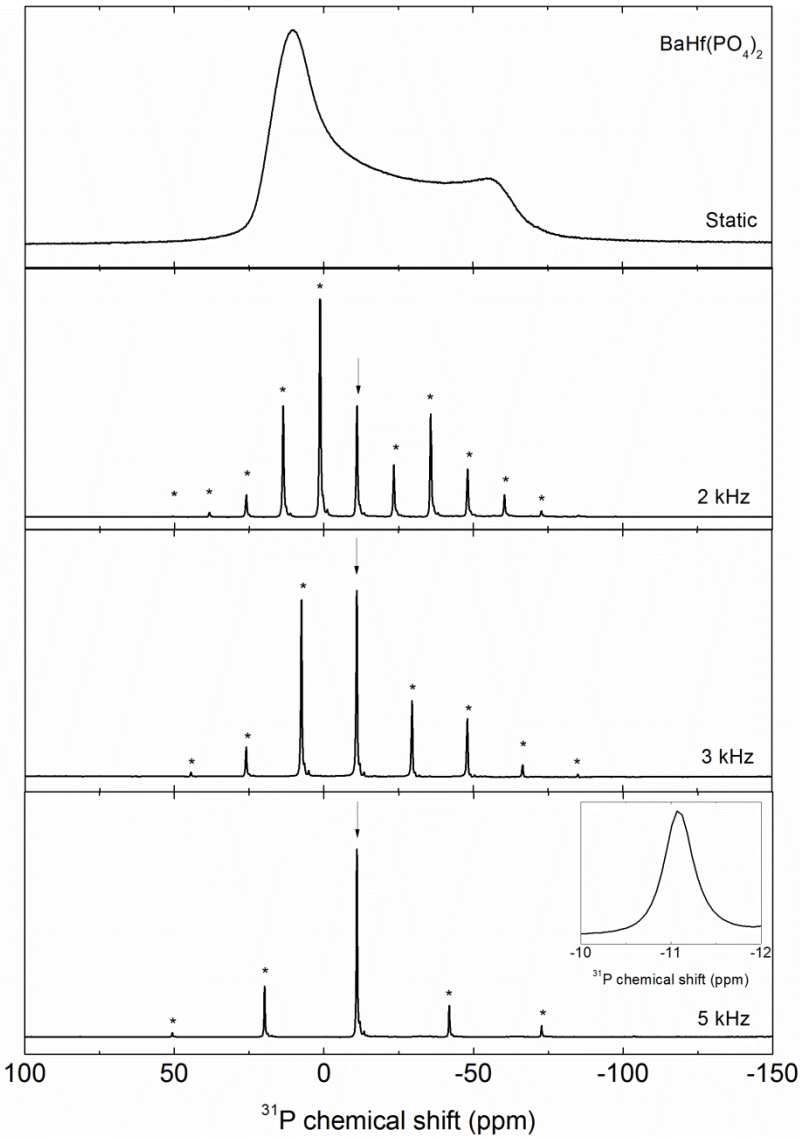

Figure 2: ^{31}P spectra of $BaHf(PO_4)_2$ acquired in static conditions and at different spinning rates. The arrow indicates the isotropic band while the stars stand for the spinning sidebands. The insert presents the central peak.

For all samples, the ^{31}P MAS NMR spectra were acquired in static conditions and at three spinning rates (2, 3 and 5 kHz). As similar data were obtained for all samples, only the $BaHf(PO_4)_2$ spectra are given in Figure 2 as example to show the spinning rate effects. Additionally, in Figure S1, the spectra of all the other $M^{II}M^{IV}(PO_4)_2$ compounds are depicted at the spinning rates of 5 and 2 kHz.

The static spectrum presents a typical CSA dominated powder pattern, and combined with slow MAS rates it has been possible to identify the isotropic bands and extract the CSA parameters. The observation of a single isotropic band for each compound is in agreement with the single P site expected from these crystalline structures. All the NMR parameters

(δ_{iso}, δ_{ii}) extracted from the spectra are gathered in Table 1. Small differences were found between static and MAS values of the CSA most probably due to ^{31}P-^{31}P coupling. These differences were accounted in the uncertainties.

Table 1: The experimental ^{31}P isotropic chemical shifts, δ_{iso}, and the anisotropic parameters (δ_{11}, δ_{22}, δ_{33}, Δ_{CSA}, η_{CSA}) of the crystalline phosphates. Each compound was attributed a random number (N°) with which it will be labelled with. Data for compounds 1-7 were obtained in the present study while for compounds 8-12 they were extracted from the literature indicated by the references.

N°	Name	δ_{iso} (ppm)	Δ_{CSA} (ppm)	η_{CSA}	δ_{11} (ppm)	δ_{22} (ppm)	δ_{33} (ppm)
1	$BaHf(PO_4)_2$	-11.1 ± 1	-53.1± 1	0.21± 0.1	21.0	9.9	-64.2
2	$BaSn(PO_4)_2$	-11.7 ± 1	-52.6± 1	0.23± 0.1	21.5	9.1	-65.7
3	$BaGe(PO_4)_2$	-21.2 ± 1	-52.6± 1	0.19± 0.1	10.1	0.1	-73.8
4	$BaZr(PO_4)_2$	-15.5 ± 1	-51.2± 1	0.21± 0.1	15.5	4.7	-66.8
5	$BaTi(PO_4)_2$	-16.1 ± 1	-50.9± 1	0.15± 0.1	13.2	5.5	-67.0
6	$CaGe(PO_4)_2$	-17.6 ± 1	-64.3± 1	0.17± 0.1	20.0	9.1	-81.9
7	β-$SrGe(PO_4)_2$	-19 ± 1	-58.9± 1	0.15± 0.1	14.9	6.0	-77.9
8	$Si_5O(PO_4)_6$	-44.1± 1[43]*	39.6	0.5	-73.6	-53.8	-4.5
9	$Ge_5O(PO_4)_6$	-32.9± 1[44]*	--	--	--	--	--
10	$LaPO_4$	-4.4± 1[38,39]*	19.3	0.75	-21.2	-6.7	15
11	$AlPO_4$	-25.9[25]/26.3± 1[83]*	--	--	--	--	--
12	$AlPO_4$-c	-30.7± 1[42]*	--	--	--	--	--

*the uncertainties are not given in the following papers, but deduced from the spectra.

3.3. *Effect of DFT optimisation on the crystalline structures*

Computed parameters often suffer from experimental errors intrinsically as the experimental crystalline structures are more representative of a thermal average than the true local environment.[51,89] To overcome this drawback, the optimisation of the atomic positions and/or the unit cell parameters is often done. To render these effects the different optimisation procedures are discussed in the following paragraph. Additionally, due to the small range of the ^{31}P δ_{iso} values (~10 ppm) in this phosphate series, we also considered the chemical shifts (Table 1) of previously published crystalline compounds (denoted thereafter as M'PO_4 as they possess only one metal cation, M') which, conveniently, have a single crystallographic P site: $Ge_5O(PO_4)_6$[44] (R-3 H[79]), $Si_5O(PO_4)_6$[43,80] (R -3 H[81]), $AlPO_4$[42] (P 3_1 2 1[82]), $AlPO_4$[42] (C 2 2 2_1[83]) and $LaPO_4$[38, 39] (P 1 2 1/a 1[84]). This approach is similar to the work done by several other authors[85,86] as it gives an overview over a broader range of chemical shifts.

In the present study three different optimisation approaches have been used: *i)* the atomic position optimisation (APO) in which only the atom positions are relaxed, *ii)* the full optimisation (FO) in which both the atom positions and cell parameters are relaxed and *iii)* full optimisation followed by scaling of the obtained structure back to the original experimental cell parameters (FOS). This last approach can be particularly advantageous in the case of the PBE GGA functional, which is known to lead to an increase of the cell dimension (by typically few %) and therefore a rescaling sometimes improves the σ_{iso}.[87,88]

In the assessment of the optimisation effects and how it will later influence the computed shielding, we considered three averaged structural parameters: *i)* the phosphorus-oxygen bond distance ($<r_{P\text{-}O}>$), *ii)* the metal-oxygen bond distance ($<r_{M\text{-}O}>$, M = M', M^{II}, M^{IV}) and, *iii)* the metal-oxygen-phosphorus bond angle ($<\theta_{M\text{-}O\text{-}P}>$, M = M', M^{II}, M^{IV}). To compare the optimized (Opt) values with those of the experimental structure (ES) we considered the following classical statistics:

$$\frac{\Delta<r_{P-O}>}{<r_{P-O}>_{ES}} = \frac{<r_{P-O}>_{Opt}-<r_{P-O}>_{ES}}{<r_{P-O}>_{ES}} * 100 \quad (1)$$

$$\frac{\Delta<r_{M-O}>}{<r_{M-O}>_{ES}} = \frac{<r_{M-O}>_{Opt}-<r_{M-O}>_{ES}}{<r_{M-O}>_{ES}} * 100 \quad (2)$$

$$\frac{\Delta<\theta_{M-O-P}>}{<\theta_{M-O-P}>_{ES}} = \frac{<\theta_{M-O-P}>_{Opt}-<\theta_{M-O-P}>_{ES}}{<\theta_{M-O-P}>_{ES}} * 100 \quad (3)$$

where Opt = APO, FO, FOS and M = M', M^{II}, M^{IV}.

The results from Equation 1 are presented in Figure S2. The $<r_{P\text{-}O}>$ data of $BaHf(PO_4)_2$ and $Si_5O(PO_4)_6$ are mostly influenced by structure optimisation with deviation from the ES values of ~6%. It is interesting to note that the optimisation effects with the FO and APO approaches lead to quite similar $<r_{P\text{-}O}>$ values. In Figure S3, the optimisation effects on the average metal-oxygen distances $<r_M^{II}{}_{\text{-}O}>$, $<r_M^{IV}{}_{\text{-}O}>$ and $<r_{M'\text{-}O}>$ are depicted as obtained using Equation 2. With ~4%, $<r_M^{IV}{}_{\text{-}O}>$ for $BaGe(PO_4)_2$ and $<r_{M'\text{-}O}>$ for $Ge_5O(PO_4)_6$ represent the largest differences compared to the ES values. Finally, Figure S4 shows the optimisation effects on the bond angles (Equation 3). The largest deviations from the ES values are again observed for $BaHf(PO_4)_2$ independent from the optimisation approach used. This analysis underlines errors more specifically in the experimental structural data of $BaHf(PO_4)_2$.

3.4. Calculation of chemical shieldings

3.4.1. The periodic calculations

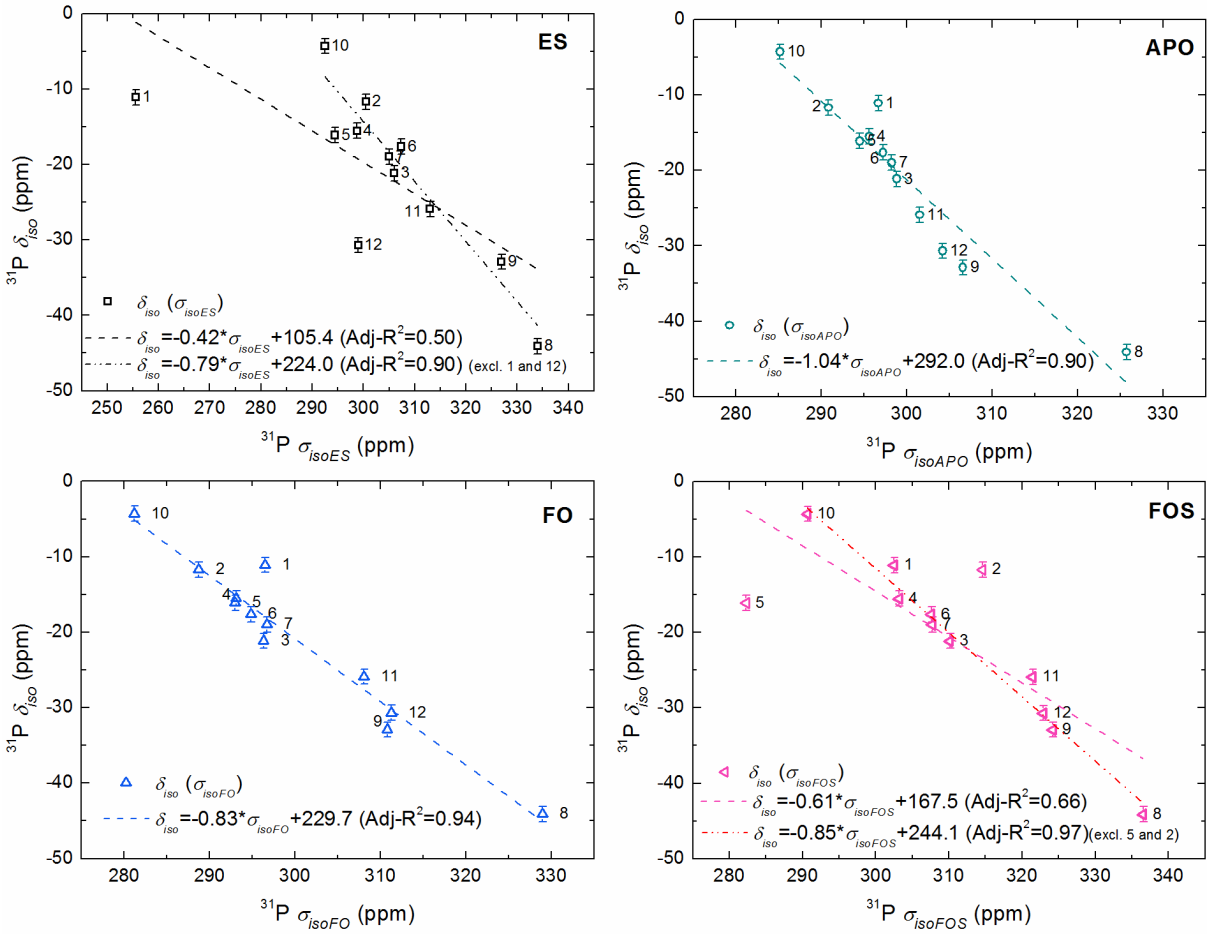

Figure 3: Plot of the experimental ^{31}P δ_{iso} against the calculated ^{31}P σ_{iso} obtained from periodic calculations. "excl." means excluding extremely deviating σ_{iso} data (see text). For the compound numbers see Table 1.

In Figure 3, the experimental δ_{iso} are plotted against the theoretical σ_{iso} data. The corresponding values are given in Table S4. As the two parameters are related through the relation[51,] $\delta_{iso} = \sigma_{ref} + a\sigma_{iso}$ (with a being the slope and σ_{ref} the "reference" shielding from the fittings), the data can be fitted using a linear equation. Among the σ_{iso} values based on the ES structures a few large deviations can be observed from the regression line fitted to all the data. The largest σ_{iso} deviations belong to $BaHf(PO_4)_2$ and $AlPO_4$-c. Indeed, after removing these values from the fit, an improvement of the linear relationship measured by the adjusted R-squared (*Adj-*R^2) was obtained as it increased from 0.50 to 0.90. The former very poor *Adj-*R^2 reflects the deficiencies of the ES parameters as already discussed by other authors.[51,89] The above situation can be improved by quantum chemical geometry optimisation which can (partly) correct the experimental errors.[51] There are a few optimisation procedures for that purpose. In the present study we probed three procedures (APO, FO and FOS), introduced in section 3.3. For the σ_{iso} data determined using the optimized crystalline structures we obtained a considerable improvement of the correlations between the δ_{iso} and the σ_{iso} values (Figure 3), particularly on the basis of the APO and FO structures (Adj-R^2 equal to 0.90 and 0.94 respectively). $BaHf(PO_4)_2$ and $AlPO_4$-c present now isotropic shieldings more in line with the others. These better correlations can indeed be traced back to the improved structural parameters of the APO and FO structures with respect to ES (Figure S2-Figure S4). $BaHfPO_4$ is the most demonstrative example, as here large changes occurred in all structural parameters upon optimisation compared to the ES.

Contrary to the two above used procedures, the FOS method does not seem to improve significantly the general correlation compared to ES (Adj-R^2=0.66 vs Adj-R^2=0.50). This is mostly due to the σ_{iso} values of $BaTi(PO_4)_2$ and $BaSn(PO_4)_2$ which deviate considerably from the fitted line. Removing their σ_{iso} values from the plot lead to an increase of *Adj-*R^2 from 0.66 to 0.97. For $BaTi(PO_4)_2$, it is the $<\theta_M{}^{IV}{}_{-OP}>$ parameter which seems to be too underestimated. After FO, the unit-cell parameters of $BaTi(PO_4)_2$ decreases from 1115.4 to 1056.4 a.u.^{3} contrary to the other unit cells which are increasing. Therefore, rescaling the optimized cell parameters to the original experimental ones worsened considerably the

achievements of the FOS. For $BaSn(PO_4)_2$, we believe that, the error of FOS might be the result of the optimisation headed towards a different local minimum.

It is also noteworthy that both *a* and σ_{ref} vary slightly, depending on the type of structure used to calculate σ_{iso}. This is the consequence of the shielding being sensitive to small changes in structural parameters. In fact, Vasconcelos et al.[85] have already reported such behaviour in phosphate based materials underlining the difficulty to choose a uniform σ_{ref}. Also, while the ideal slope must be -1, nuclear quantum effects, incomplete basis sets, and other systematic errors in the DFT calculations can lead to deviations from this ideal value.[90]

3.4.2. Small clusters approach

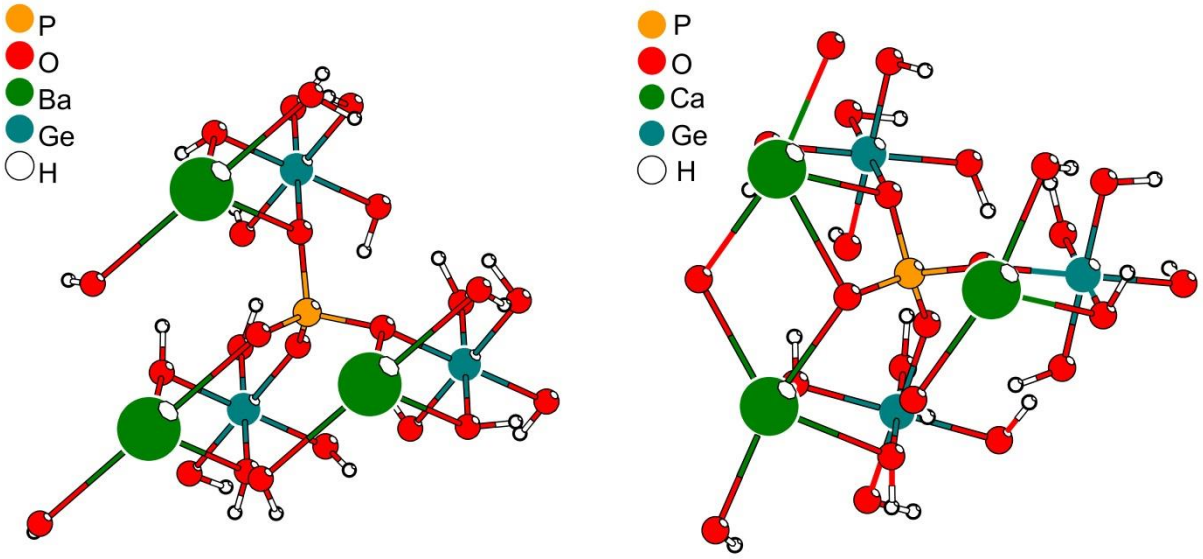

Figure 4: A typical cluster model structure used for the calculations of $M^{II}M^{IV}(PO_4)_2$ yavapaiite (left) and low-yavapaiite (right). More details are given in the Supporting Information.

As examples for our cluster models for the yavapaiite and low-yavapaiite structures, the clusters for $BaGe(PO_4)_2$ and $CaGe(PO_4)_2$, respectively, are shown in Figure 4. The cores of the clusters consist of atoms, up to the third coordination shell (PO_4, metals, oxygens), taken from the ES and FO structures. The choice for FO from the three solid-state optimized structure types is reasoned by the found best linear correlation between δ_{iso} and σ_{iso}. The hydrogen atoms were added to the terminal oxygen atoms in order to compensate for the very large negative charges of the core structures. The final charges of our clusters were -5 e except for Al and La with charges of -3 e. The strain due to the manually added hydrogens was removed by partial geometry optimisations, in which the hydrogen atoms were subjected

to geometry optimisation while the core of the cluster was kept fixed. Test calculations by varying the hydrogen bonding pattern around the fixed cores revealed only a slight influence (up to 2 ppm) on the calculated ^{13}P shieldings. The present reported cluster sizes were most suitable for the description of the NMR properties of the target compounds as reducing them to the second coordination shell resulted in unreliable chemical shieldings while expanding them led to serious SCF convergence problems. The exact compositions and pictures of the clusters together with the Cartesian coordinates of the final structures are given in the Supplementary Information.

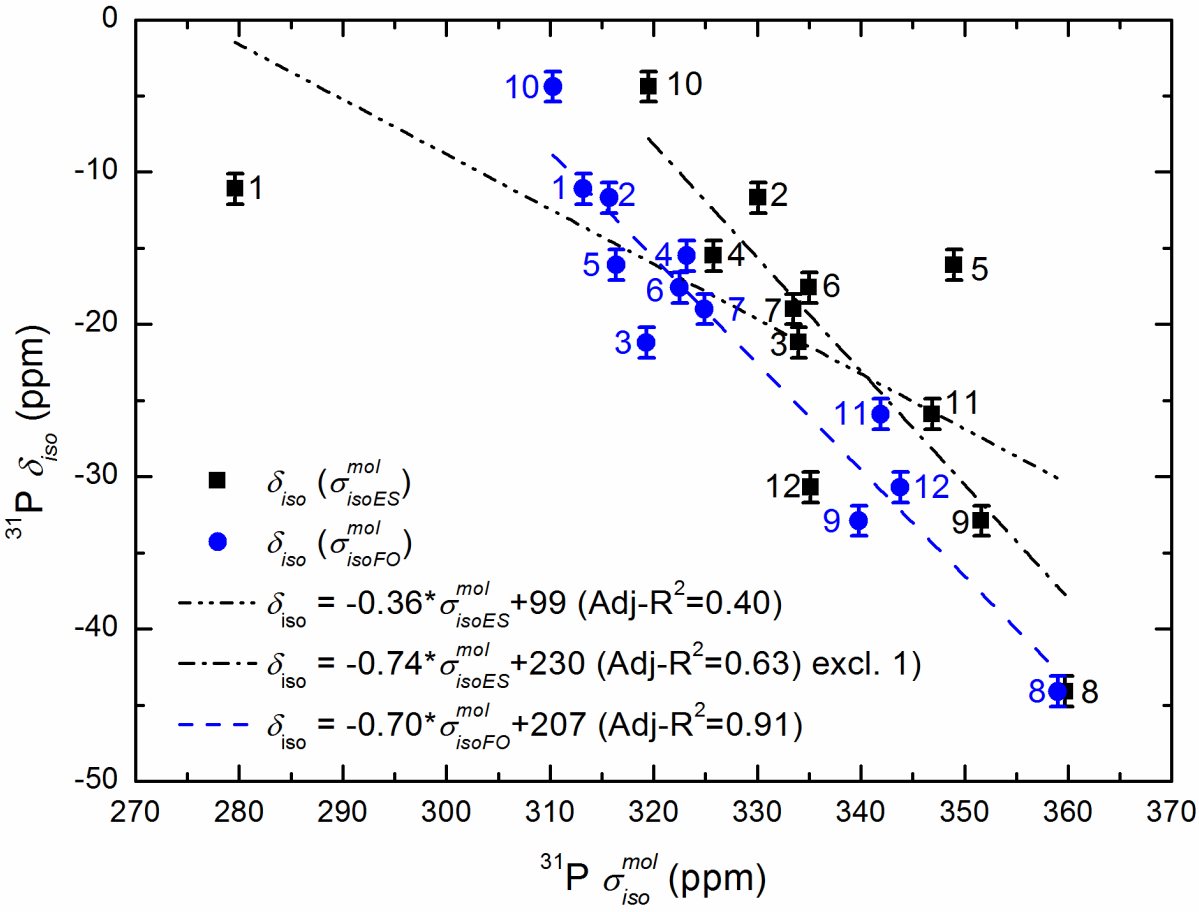

Figure 5: Plot of the experimental ^{31}P δ_{iso} against the calculated ^{31}P σ_{iso}^{mol} obtained based on the cluster models. For the compound numbers see Table 1.

In Figure 5 the experimental δ_{iso} values are plotted against the theoretical shielding (σ_{iso}^{mol}) obtained from our cluster models.

The corresponding values are given in Table S5. Similarly to the solid-state calculations, the δ_{iso} vs σ_{isoES}^{mol} have a poor correlation due mainly to the above shown error in the

283 experimental structural data of $BaHf(PO_4)_2$. The correlation is thus improved from Adj-R^2 =
284 0.40 to 0.63 after omitting its chemical shielding. Using the clusters based on the FO
285 structures, the σ_{isoFO}^{mol} data correlate now well with δ_{iso} with an Adj.-R^2 equal to 0.84. This
286 result reflects the efficiency of using small molecular cluster models to represent the solid-
287 state, as already shown by some authors in other phosphate series[85,91].

288 To go beyond these two classical approaches (*i.e.* periodic and cluster) and to capture the
289 full periodic nature of the crystal while also obtaining the higher accuracy associated with
290 computational models, we applied the new method recently suggested by Dračínský et al.[92]. It
291 consists in correcting the GIPAW calculated shieldings (σ_{corr}) by considering the difference
292 between the shielding calculated with the B3LYP and the PBE functionals employed in the
293 GIPAW calculation. For our study, we considered the FO structure and applied the following
294 equation:

295 $$\sigma_{corr} = \sigma_{cryst}^{GIPAW} - \sigma_{mol}^{PBE} + \sigma_{mol}^{B3LYP} \quad (4)$$

296 with σ_{cryst}^{GIPAW} corresponding to the σ_{isoFO} obtained using the GGA-based GIPAW method
297 and; σ_{mol}^{PBE} and σ_{mol}^{B3LYP} corresponding to the σ_{isoFO}^{mol} obtained based on the clusters using the
298 PBE (same GGA as the GIPAW calculation) and B3LYP (hybrid) functionals.
299

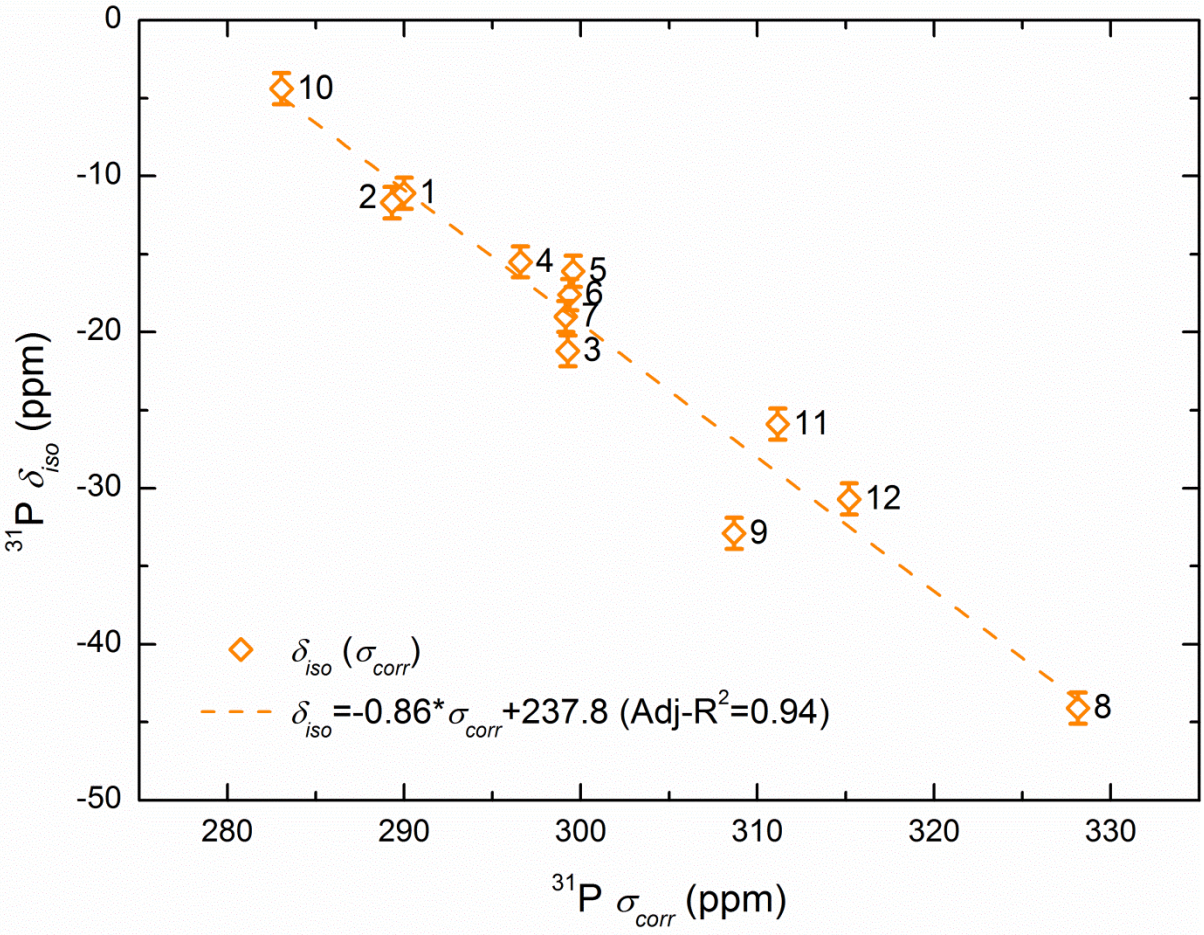

Figure 6: Plot of the experimental ^{31}P δ_{iso} against the calculated ^{31}P σ_{corr} obtained based on equation 4. For the compound numbers see Table 1.

In Figure 6, we plotted the experimental δ_{iso} values against the corrected shielding. The first observation is an increase of the linear slope from -0.83 to -0.86 which is positively getting closer to the ideal value of -1. In Table 2, we determined the theoretical δ_{iso} values based on the GIPAW and Dračínský approaches. This allows to easily compare them with the experimental values. The lowest mean absolute error (MAE) is obtained for the corrected shielding values confirming again that this method does lead to data improvements. The maximal absolute error for δ_{corr} of 6 ppm is obtained for $Ge_5O(PO_4)_6$. Nonetheless, this value also corresponds to an improvement from the non-corrected shielding (decrease of about 2 ppm). It is worth mentioning that this theoretical δ_{iso} is not well represented independently of the type of calculations approach or optimization considered. This might imply a larger error of the δ_{iso} value. It is also interesting to notice that the shielding of $BaHf(PO_4)_2$ is specifically improved with this correction most probably implying the problems in GGA-PBE in addition to the structural parameter errors previously discussed.

Table 2: Theoretical δ_{iso} in ppm with $\delta_{cryst}^{GIPAW} = -0.83 * \sigma_{cryst}^{GIPAW} + 229.7$ and $\delta_{corr} = -0.86 * \sigma_{corr} + 237.8$. The MAE and maximal absolute errors (ppm) are also given.

N°	Name	δ_{cryst}^{GIPAW}	δ_{corr}

1	$BaHf(PO_4)_2$	-16.8	-10.9
2	$BaSn(PO_4)_2$	-11.5	-10.3
3	$BaGe(PO_4)_2$	-17.8	-18.9
4	$BaZr(PO_4)_2$	-15.0	-16.6
5	$BaTi(PO_4)_2$	-17.8	-19.1
6	$CaGe(PO_4)_2$	-16.6	-18.9
7	β-$SrGe(PO_4)_2$	-18.1	-18.8
8	$Si_5O(PO_4)_6$	-45.0	-43.6
9	$Ge_5O(PO_4)_6$	-41.0	-26.9
10	$LaPO_4$	-5.2	-5.0
11	$AlPO_4$	-27.6	-29.0
12	$AlPO_4$-c	-30.3	-32.5
	MAE	2.1	1.8
	Max. Abs. Err.	8.1	6.0

3.4.3. *Chemical shift shieldings*

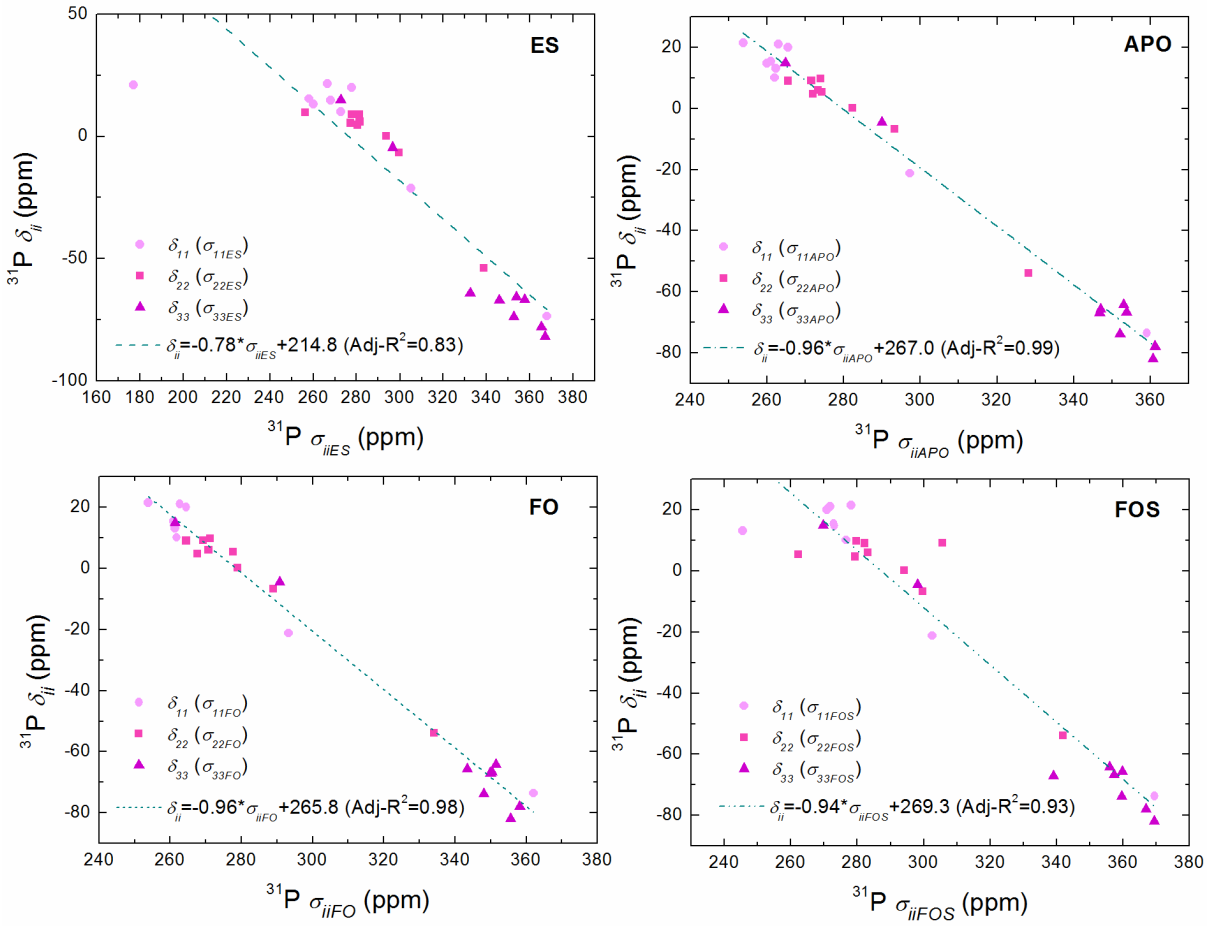

Figure 7: Plot of the experimental δ_{ii} against the calculated σ_{ii} values and their corresponding fits (dashed lines).

The σ_{ii} values correspond to the eigenvalues of the chemical shielding tensor which is a 3 x 3 matrix in the laboratory frame[93,94]:

$$\boldsymbol{\sigma}_{lab} = \begin{pmatrix} \sigma_{xx} & \sigma_{xy} & \sigma_{xz} \\ \sigma_{yx} & \sigma_{yy} & \sigma_{yz} \\ \sigma_{zx} & \sigma_{zy} & \sigma_{zz} \end{pmatrix}$$

The chemical shielding tensor and the associated σ_{ii} values are given as part of the QE output file. We noticed that contrary to the good results on δ_{iso} vs σ_{iso}, the σ_{ii} from the output files gave a poorer linear correlation with the δ_{ii} as shown in Figure S5. We checked the eigenvalues by recalculating them with the Mathematica software® and the results are shown in Figure 7. One can notice that a much better overall correlation is now obtained with Adj-R^2 coefficient improved from 0.25 to 0.83 for the ES, 0.92 to 0.99 for the APO, 0.93 to 0.98 for the FO and, 0.87 to 0.93 for the FOS. These differences suggest an erroneous determination of the eigenvalues in the QE code. We also show here that both slope and σ_{ref} are dependent upon the type of optimisation.

In the literature, while most review papers[51,43] suggest to plot δ_{ii} vs σ_{ii}, as done in the present work, some authors prefer the σ_{ii} vs δ_{ii} representation as a slope of -1 is most easily obtained. We therefore gave in Table 3 the values of the linear relations $\sigma_{ii} = \sigma_{iiref} + b*\delta_{ii}$ in order to compare with the published data. Holmes et al.[91] found a linear correlation of $\sigma_{ii} = -1.09*\delta_{ii}+270$ for a set of 57 compounds and our results are in line with their observations.

Table 3: Linear fit considering $\sigma_{ii} = \sigma_{iiref} + b*\delta_{ii}$.

Opt.	*b*	σ_{iiref}	R^2
ES	-1.1	280.1	0.83
ES excl. 1	-1.0	286.2	0.97
APO	-1.03	279.6	0.99
FO	-1.03	278.4	0.98
FOS	-0.99	288.4	0.93
FOS excl. 5	-0.98	291.5	0.97

4. Conclusion

We studied here the local P environment in a series of crystalline phosphates by combing ^{31}P NMR with periodic and small cluster DFT calculations. All the ^{31}P spectra acquired

possess a good resolution with a clear identification of a single P signal in agreement with their crystallographic structures. Using the GIPAW approach, optimisations of the crystalline structure parameters using three types approaches (APO, FO and FOS) led to an overall improvement of the calculated NMR parameters, especially for $BaHf(PO_4)_2$. Good linear correlations, δ_{iso} vs σ_{iso}, were achieved with both APO (*Adj-*R^2=0.90) and FO (*Adj-*R^2=0.94) structures, with a preference on the latest optimisation approach. Using the ES and FO structures, small cluster models were constructed. The isotropic chemical shielding (σ_{iso}^{mol}) extracted presented a good correlation with the isotropic chemical shifts. This underlines the efficiency of such clusters and its eventual use as substitute to model the infinite crystal especially in the case of paramagnetic systems. Nonetheless, a better improvement of the theoretical isotropic chemical shift was achieved by combining the advantages of both plane-wave and molecular computational approaches (MAE decreasing from 2.1 to 1.8). For the CSA parameters, good linear correlations were also obtained between the δ_{ii} and the σ_{ii} data determined on the basis of the APO (*Adj-*R^2=0.99) and FO (*Adj-*R^2=0.98) relaxed structures, with this time slightly better results with the first optimisation approach. The present paper show a first step in the NMR study of $M^{II}M^{IV}(PO_4)_2$ compounds using periodic and cluster calculations with an extension to any phosphates.

366 **References**

1 E. Morin, G. Wallez, S. Jaulmes, J. C. Couturier, M. Quarton, *J. Solid State Chem.* 137 (1998) 283–288, https://doi.org/10.1006/jssc.1997.7735.

2 K. Fukuda, A. Moriyama, T. Iwata, *J. Solid State Chem.* 178 (2005) 2144–2151, https://doi.org/10.1016/j.jssc.2005.04.022.

3 G. Blasse, G. J. Dirksen, *Chem. Phys. Lett.* 62 (1979) 19-20, https://doi.org/10.1016/0009-2614(79)80403-0.

4 C. R. Miao, C. C. Torardi, *J. Solid State Chem.* 155 (2000) 229-232, https://doi.org/10.1006/jssc.2000.8938.

5 Z. J. Zhang, J. L. Yuan, X. J. Wang, D. B. Xiong, H. H. Chen, J. T. Zhao, Y. B. Fu, Z. M. Qi, G. B. Zhang, C. S. Shi, *J. Phys. D: Appl. Phys.* 40 (2007) 1910–1914, https://doi.org/10.1088/0022-3727/40/7/012.

6 B. Yan, J. Gu, X. Xiao, *J. Nanopart. Res.* 12 (2010) 2145–2152, https://doi.org/10.1007/s11051-009-9776-x.

7 X. Xiao, B. Yan, *J. Amer. Ceram. Soc.* 93 (2010) 2195–2201, https://doi.org/10.1111/j.1551-2916.2010.03716.x.

8 R. R Parrish, *Canadian Journal of Earth Science* 27 (1990) 1431–1450, https://doi.org/10.1139/e90-152.

9 J.-M. Montel, S. Foret, M. Veschambre, C. Nicollet, A. Provost, *Chemical Geology* 131 (1996) 37-53, https://doi.org/10.1016/0009-2541(96)00024-1.

10 V. Brandel, N. Dacheux, E. Pichot, M. Genet, J. Emery, J. Y. Buzare, R. Podor, *Chem. Mater.* 10 (1998) 345–350, https://doi.org/10.1021/cm970513d.

11 O. Terra, N. Dacheux, F. Audubert, R. Podor, *J. Nuc. Mater.* 352 (2006) 224-232, https://doi.org/10.1016/j.jnucmat.2006.02.058.

12 O. Terra, N. Clavier, N. Dacheux, R. Podor, *New J. Chem.* 27 (2003) 957-967, https://doi.org/10.1039/B212805P.

13 D. M. Bykov, A. I. Orlova, S. V. Tomilin, A. A. Lizin, A. N. Lukinykh, *Radiochemistry* 48 (2006) 234–239, https://doi.org/10.1134/S1066362206030052.

14 D. Bregiroux, O. Terra, F. Audubert, N. Dacheux, V. Serin, R. Podor, D. Bernache-Assollant, *Inorg. Chem.* 46 (2007) 10372-10382, https://doi.org/10.1021/ic7012123.

15 P. Sengupta, *J. Hazard. Mater.* 235-236 (2012) 17-28, https://doi.org/10.1016/j.jhazmat.2012.07.039.

16 I. W. Donald, B. L. Metcalfe, R. N. J. Taylor, *J. Mater. Sci.* 32 (1997) 5851-5887, https://doi.org/10.1023/A:1018646507438.

17 W. E. Lee, M. I. Ojovan, M. C. Stennett, N. C. Hyatt, *Adv. Appl. Ceram.* 105 (2006) 3-12, https://doi.org/10.1179/174367606X81669.

18 K. Popa, D. Bregiroux, R. J. M. Konings, A. F. Popa, T. Gouder, T. Geisler, P. E. Raison, *J. Solid State Chem.* 180 (2007) 2346–2355, https://doi.org/10.1016/j.jssc.2007.06.006.

19 S. Neumeier, Y. Arinicheva, Y. Ji, J. M. Heuser, P. M. Kowalski, P. Kegler, H. Schlenz, D. Bosbach, G. Deissmann, *Radiochim. Acta* 105 (2017) 961-984, https://doi.org/10.1515/ract-2017-2819.

20 K. Popa, R. J. M. Konings, T. Wiss, H. Leiste, *J. Radioanal. Nucl. Chem.* 273 (2007) 563-567, https://doi.org/10.1007/s10967-007-0910-x.

21 K. Popa, T. Shvareva, L. Mazeina, E. Colineau, F. Wastin, R.J.M. Konings, A. Navrotsky, Am. Mineral. 93 (2008) 1356-1362, https://doi.org/10.2138/am.2008.2794

22 Y. Arinicheva, K. Popa, A.C. Scheinost, A. Rossberg, O. Dieste Blanco, P.E. Raison, A. Cambriani, J. Somers, D. Bosbach, S. Neumeier, *J. Nucl. Mater.*, 493 (2017) 404-411, https://doi.org/10.1016/j.jnucmat.2017.06.034.

23 D. Bregiroux, K. Popa, G.Wallez, *J. Solid State Chem.* 230 (2015) 26-33, https://doi.org/10.1016/j.jssc.2015.06.010.
24 D. Bregiroux, G. Wallez, K. Popa, *Solid State Sci.* 41 (2015) 43-47, http://dx.doi.org/10.1016/j.solidstatesciences.2015.02.004.
25 A. K. Cheetham, N. J. Clayden, C. M. Dobson, R. J. B. Jakeman, *J. Chem. Soc., Chem. Commun.*, 1986, 195-197, https://doi.org/10.1039/C39860000195.
26 I. D. Brown, R. D Shannon, *Acta Cryst.* A29 (1973) 266-282, https://doi.org/10.1107/S0567739473000689.
27 A. C. Palke, J. F. Stebbins, *Am. Miner.* 96 (2011) 343-353, https://doi.org/10.2138/am.2011.3816.
28 A. C. Palke, J. F. Stebbins, L. A. Boatner, *Inorg. Chem.* 52 (2013) 12605-12615, https://doi.org/10.1021/ic401757z.
29 L. Martel, J.-F. Vigier, D. Prieur, S. Nourry, A. Guiot, K. Dardenne, J. Boshoven, J. Somers, *J. Phys. Chem. C* 118 (2014) 27640−27647, https://doi.org/10.1021/jp507088t.
30 F. Gendron, K. Sharkas, J. Autschbach, *J. Phys. Chem. Lett.* 6 (2015) 2183−2188, https://doi.org/10.1021/acs.jpclett.5b00932.
31 F. Gendron, B. Pritchard, H. Bolvin, J. Autschbach, *Inorg. Chem.* 53 (2014) 8577–8592, https://doi.org/10.1021/ic501168a.
32 D. E. Smiles, G. Wu, P. Hrobárik, T. W. Hayton, *J. Am. Chem. Soc.* 138 (2016) 814−825, https://doi.org/10.1021/jacs.5b07767.
33 L. Martel , A. Rakhmatullin, J. J. Baldoví, M. Perfetti, K. Popa, M. Deschamps, T. Gouder, E.Colineau, A. Kovács, J.-C. Griveau, *Phys. Rev. B* 100 (2019) 054412, https://doi.org/10.1103/PhysRevB.100.054412.
34 A. Mondal, M. W. Gaultois, A. J. Pell, M. Iannuzzi, C. P. Grey, J. Hutter, M. Kaupp, *J. Chem. Theory Comput.*, 14 (2018) 377−394.
35 E. J. Graeber, A. Rosenzweig, *Am. Miner.* 56 (1971) 1917–1933.
36 J. W. Anthony, W. J. McLean, *Am. Miner.* 57 (1972) 1546–1549.
37 K. Popa, G. Wallez, D. Bregiroux, P. Loiseau, *J. Solid State Chem.* 184 (2011) 2629-2634, https://doi.org/10.1016/j.jssc.2011.07.037.
38 D. Bregiroux, F. Audubert, T. Charpentier, D. Sakellariou, D. Bernache-Assollant, *Solid State Sci.* 9 (2007) 432-439, https://doi.org/10.1016/j.solidstatesciences.2007.03.019.
39 K. Popa, P. E. Raison, L. Martel, P. M. Martin, D. Prieur, P. L. Solari, D. Bouëxière, R. J. M. Konings, J. Somers, *J. Solid State Chem.* 230 (2015) 169-174, https://doi.org/10.1016/j.jssc.2015.07.002.
40 D. Müller, E. Jahn, G. Ladwig, U. Haubenreisser, *Chem. Phys. Lett.*, 109 (1984) 332−336, https://doi.org/10.1016/0009-2614(84)85596-7.
41 K. Kanehashi, T. Nemoto, K. Saito, J. Non-Cryst. Solids, 2007, **353**, 4227-4231, https://doi.org/10.1016/j.jnoncrysol.2007.05.020.
42 D. M. Dawson, S. E. Ashbrook, *J. Phys. Chem. C*, 118 (2014) 23285-23296, https://doi.org/10.1021/jp507644z.
43 C. Bonhomme, C. Gervais, C. Coelho, F. Pourpoint, T. Azaïs, L. Bonhomme-Coury, F. Babonneau, G. Jacob, M. Ferrari, D. Canet, J. R. Yates, C. J. Pickard, S.A. Joyce, F. Mauri, D. Massiot, *Magn. Reson. Chem.* 48 (2010) S86-S102, https://doi.org/10.1002/mrc.2635.
44 E. R. Losilla, A. Cabeza, S. Bruque, M. A. G. Aranda, J. Sanz, J. E. Iglesias, J. A. Alonso, *J. Solid State Chem.* 156 (2001) 213-219, https://doi.org/10.1006/jssc.2000.8984.
45 K. Popa, R. J. M. Konings, P. Boulet, D. Bouëxière, A. F. Popa, *Thermochim. Acta* 436 (2005) 51-55, https://doi.org/10.1016/j.tca.2005.06.035.
46 K. Popa, R.J.M. Konings, O. Beneš, T. Geisler, A.F. Popa, *Thermochim. Acta*, 451 (2006) 1-4, https://doi.org/10.1016/j.tca.2006.08.011.

47 T. Geisler, K. Popa, R. J. M. Konings, A. F. Popa, *J. Solid State Chem.* 179 (2006) 1490-1495, https://doi.org/10.1016/j.jssc.2006.01.065.
48 D. Massiot, F. Fayon, M. Capron, I. King, S. Le Calvé, B. Alonso, J.-O. Durand, B. Bujoli, Z. Gan, G. Hoatson, *Magn. Reson.Chem.* 40 (2002) 70-76, https://doi.org/10.1002/mrc.984.
49 P. Giannozzi, S. Baroni, N. Bonini, M. Calandra, R. Car, C. Cavazzoni, D. Ceresoli, G. L Chiarotti, M. Cococcioni, I. Dabo, A. Dal Corso, S. de Gironcoli, S. Fabris, G. Fratesi, R. Gebauer, U. Gerstmann, C. Gougoussis, A. Kokalj, M. Lazzeri, L. Martin-Samos, N. Marzari, F. Mauri, R. Mazzarello, S. Paolini, A. Pasquarello, L. Paulatto, C. Sbraccia, S. Scandolo, G. Sclauzero, A. P Seitsonen, A. Smogunov, P. Umari, R. M Wentzcovitch, *J. Phys.: Condens. Matter* 21 (2009) 395502, https://doi.org/10.1088/0953-8984/21/39/395502.
50 C. J. Pickard, F. Mauri, *Phys. Rev. B*, 63 (2001) 245101, https://doi.org/10.1103/PhysRevB.63.245101.
51 T. Charpentier, *Solid State NMR*, 40 (2011) 1−20, https://doi.org/10.1016/j.ssnmr.2011.04.006.
52 J. P. Perdew, K. Burke, M. Ernzerhof, *Phys. Rev. Lett.* 77 (1996) 3865-3868, https://doi.org/10.1103/PhysRevLett.77.3865.
53 N. Trouiller, J. Martins, *Phys. Rev. B*, 43 (1991) 1993-2006, https://doi.org/10.1103/PhysRevB.43.1993.
54 http://www.quantum-espresso.org/pseudopotentials/pslibrary/.
55 https://sites.google.com/site/dceresoli/pseudopotentials.
56 http://www.quantum-espresso.org.
57 U. Haeberlen, In Advances in Magnetic Resonance; Suppl. 1; J. S. Waugh, Ed.; Academic Press: New York, 1976.
58 M. Mehring, Principles of High Resolution NMR in Solids, 2nd. ed.; Springer Verlag: Berlin, 1983.
59 H. W. Spiess, In NMR Basic Principles and Progress; P. Diehl, E. Fluck, R. Kosfeld, Eds.; Springer Verlag, Berlin, 1978, Vol. 15.
60 M. J. Frisch, G. W. Trucks, H. B. Schlegel, G. E. Scuseria, M. A. Robb, J. R. Cheeseman, G. Scalmani, V. Barone, B. Mennucci, G. A. Petersson, H. Nakatsuji, M. Caricato, X. Li, H. P. Hratchian, A. F. Izmaylov, J. Bloino, G. Zheng, J. L. Sonnenberg, M. Hada, M. Ehara, K. Toyota, R. Fukuda, J. Hasegawa, M. Ishida, T. Nakajima, Y. Honda, O. Kitao, H. Nakai, T. Vreven, J. A. Montgomery Jr., J. E. Peralta, F. Ogliaro, M. Bearpark, J. J. Heyd, E. Brothers, K. N. Kudin, V. N. Staroverov, T. Keith, R. Kobayashi, J. Normand, K. Raghavachari, A. Rendell, J. C. Burant, S. S. Iyengar, J. Tomasi, M. Cossi, N. Rega, J. M. Millam, M. Klene, J. E. Knox, J. B. Cross, V. Bakken, C. Adamo, J. Jaramillo, R. Gomperts, R. E. Stratmann, O. Yazyev, A. J. Austin, R. Cammi, C. Pomelli, J. W. Ochterski, R. L. Martin, K. Morokuma, V. G. Zakrzewski, G. A. Voth, P. Salvador, J. J. Dannenberg, S. Dapprich, A. D. Daniels, O. Farkas, J. B. Foresman, J. V. Ortiz, J. Cioslowski, D. J. Fox, Gaussian 09, Revision D.01. Gaussian, Inc., Wallingford CT, 2010.
61 W. R. Wadt, P. J. Hay, *J. Chem. Phys.*, 82 (1985) 284, https://doi.org/10.1063/1.448800.
62 W. R. Wadt, P. J. Hay, *J. Chem. Phys.* 82 (1985) 299, https://doi.org/10.1063/1.448975.
63 A. D. Becke, *J. Chem. Phys.*, 98 (1993) 5648-5652, https://doi.org/10.1063/1.464913.
64 C. Lee, W. Yang, R. G. Parr, *Phys. Rev. B*, 37 (1988) 785-789, https://doi.org/10.1103/PhysRevB.37.785.
65 T. H. Dunning, Jr., *J. Chem. Phys.* 90 (1989) 1007, https://doi.org/10.1063/1.456153.
66 D. E. Woon and T. H. Dunning, Jr., *J. Chem. Phys.* 98 (1993) 1358, https://doi.org/10.1063/1.464303.

67 J. Koput and K.A. Peterson, *J. Phys. Chem. A* 106 (2002) 9595–9599, https://doi.org/10.1021/jp026283u.
68 A. K. Wilson, D. E. Woon, K. A. Peterson, T. H. Dunning, Jr., *J. Chem. Phys.* 110 (1999) 7667, https://doi.org/10.1063/1.478678.
69 N.B. Balabanov and K.A. Peterson, *J. Chem. Phys.* 123 (2005) 064107, https://doi.org/10.1063/1.1998907.
70 X. Cao, M. Dolg, J. Chem. Phys. 115, 7348 (2001), https://doi.org/10.1063/1.1406535.
71 X. Cao, M. Dolg, J. Molec. Struct. (Theochem) 581 (2002) 139, https://doi.org/10.1016/S0166-1280(01)00751-5.
72 M. Kaupp, P. v. R. Schleyer, H. Stoll, H. Preuss, *J. Chem. Phys.* 94 (1991) 1360, https://doi.org/10.1063/1.459993.
73 B. Metz, H. Stoll, M. Dolg, *J. Chem. Phys.* 113 (2000) 2563, https://doi.org/10.1063/1.1305880.
74 K. A. Peterson, *J. Chem. Phys.* 119 (2003) 11099, https://doi.org/10.1063/1.1622923.
75 K. A. Peterson, D. Figgen, M. Dolg, H. Stoll, *J. Chem. Phys.* 126 (2007) 124101, https://doi.org/10.1063/1.2647019.
76 D. Figgen, K.A. Peterson, M. Dolg, H. Stoll, *J. Chem. Phys.* 130 (2009) 164108, https://doi.org/10.1063/1.3119665.
77 J. R. Cheeseman, G. W. Trucks, T. A. Keith, M. J. Frisch, *J. Chem. Phys.* 104 (1996) 5497-5509, https://doi.org/10.1063/1.471789.
78 D. Bregiroux, K. Popa, R. Jardin, P. E. Raison, G. Wallez, M. Quarton, M. Brunelli, C. Ferrero, R. Caciuffo, *J. Solid State Chem.* 182 (2009) 1115-1120, https://doi.org/10.1016/j.jssc.2009.02.012.
79 H. Mayer, H. Völlenkle, *Monatsh. Chem.* **103** (1972) 1560.
80 C. Coelho, T. Azais, L. Bonhomme-Coury, G. Laurent, C. Bonhomme, *Inorg. Chem.* 46 (2007) 1379-1387, https://doi.org/10.1021/ic061964f.
81 H. Mayer, Monatshefte Chem. 105 (1974) 46-54, https://doi.org/10.1007/BF00911286.
82 H. N. Ng, C. Calvo, *Can. J. Phys.* 54 (1976) 638- 647, https://doi.org/10.1139/p76-070.
83 B. L. Phillips, J. G. Thompson, Y. Xiao, R. J. Kirkpatrick, *Phys. Chem. Miner.* 20 (1993) 341-352, https://doi.org/10.1007/BF00215105.
84 S. Jaulmes, *Bull. Soc. fr. Minéral. Cristallog*. 95 (1972) 42-46.
85 F. Vasconcelos, S. Cristol, J.-F. Paul, L. Montagne, F. Mauri, L. Delevoye, *Magn. Reson. Chem.* 48 (2010) S142-S150, https://doi.org/10.1002/mrc.2667.
86 K. Pilar, Z. Deng, M. B. Preefer, J. A. Cooley, R. Clément, R. Seshadri, A. K. Cheetham, Phys. Chem. Chem. Phys. 21 (2019) 10070-10074, https://doi.org/10.1039/c9cp01420a.
87 T. Charpentier, S. Ispas, M. Profeta, F. Mauri, C. J. Pickard, *J. Phys. Chem. B* 108 (2004) 4147-4161, https://doi.org/10.1021/jp0367225.
88 M. Profeta, F. Mauri, C. J. Pickard, *J. Am. Chem. Soc.* 125 (2003) 541-548, https://doi.org/10.1021/ja027124r.
89 J. R. Yates, S. E. Dobbins, C. J. Pickard, F. Mauri, P. Y. Ghi, R. K. Harris, *Phys. Chem. Chem. Phys.*7 (2005) 1402-1407, https://doi.org/10.1039/B500674K.
90 M. Dračínský, P. Hodgkinson, *Chem. Eur. J.*, 20 (2014) 2201–2207, https://doi.org/10.1002/chem.201303496.
91 S. T. Holmes, R. J. Iuliucci, K. T. Mueller, C. Dybowski, *J. Chem. Theory Comput.* 11 (2015) 5229−5241, https://doi.org/10.1021/acs.jctc.5b00752
92 M. Dračínský, P. Unzueta, G. J. O. Beran, *Phys. Chem. Chem. Phys.*, 21 (2019) 14992, https://doi.org/10.1039/c9cp01666j.
93 R. P. Young, C. R. Lewis, C. Yang, L. Wang, J. K. Harper, L. J. Mueller, *Magn Reson Chem.* 57 (2019) 211–223, https://doi.org/10.1002/mrc.4793

94 L. J. Mueller, *Concept. Magn. Reson. A*, 38 (2011) 221–235, https://doi.org/10.1002/cmr.a.20224